OPEN ACCESS

Geographical Sciences ARTICLE

Urbanization and climate change disproportionately affect worldwide rooftop solar viability for self-sufficient electricity

Jing Chen,[1] Yimin Chen,[1,*] Ming Luo,[1] Yuanzhi Yao,[2,*] Xiaocong Xu,[1] Weilin Liao,[1] Xiaoping Liu,[1,*] and Xia Li[2]

*Correspondence: chenym49@mail.sysu.edu.cn (Y.C.); yzyao@geo.ecnu.edu.cn (Y.Y.); liuxp3@mail.sysu.edu.cn (X.P.L.)

Received: October 15, 2025; Accepted: April 9, 2026; Published Online: April 17, 2026; https://doi.org/10.59717/j.xinn-geo.2026.100222

GRAPHICAL ABSTRACT

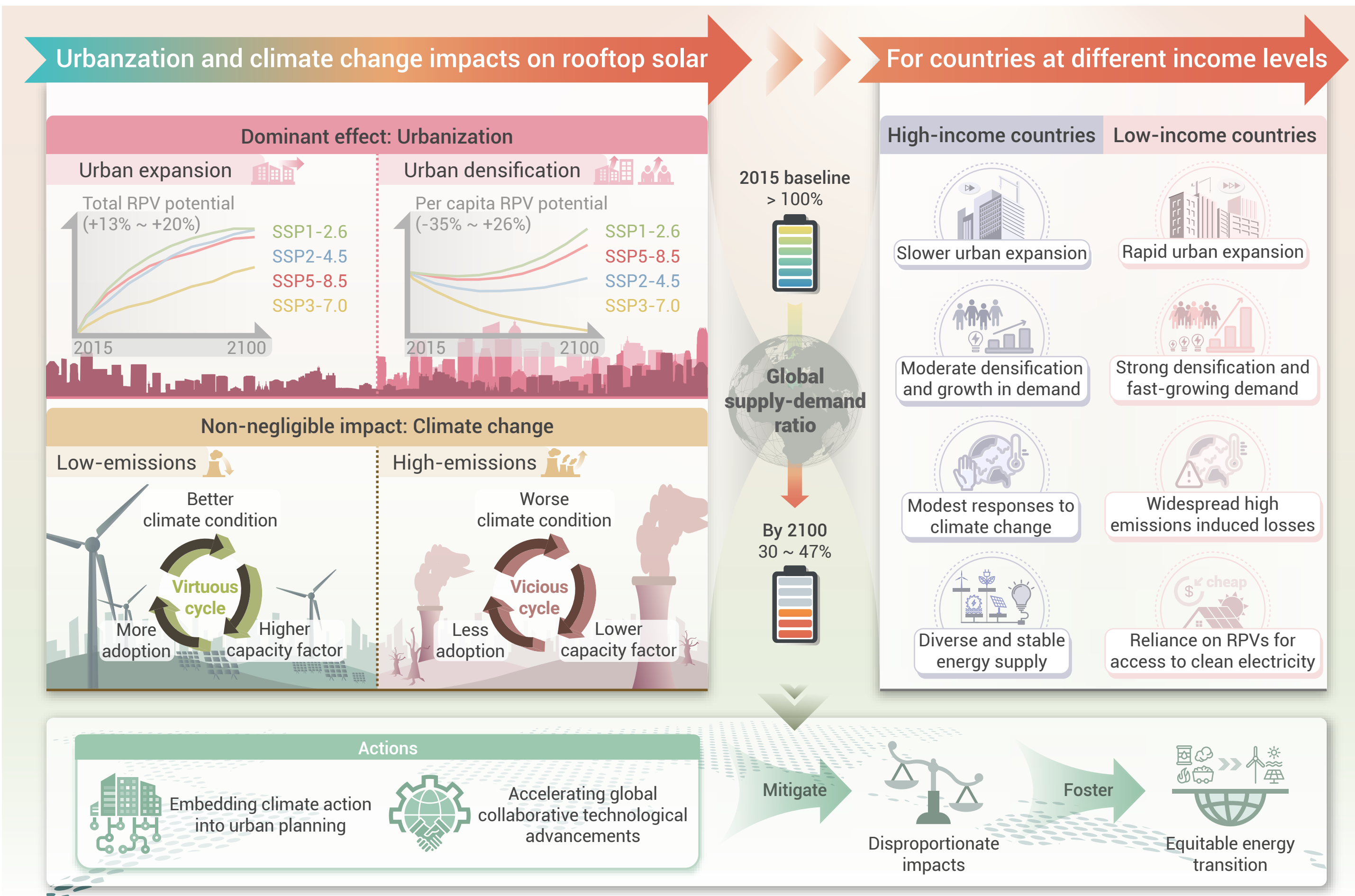

PUBLIC SUMMARY

- Urban expansion will considerably increase rooftop photovoltaic (RPV) potential over the 21st century.
- Per capita RPV potential is likely to decline due to the prevailing trend towards urban densification.
- Urbanization primarily drives RPV potential changes, but climate change impacts cannot be overlooked.
- Urbanization and climate change may disproportionately constrain lower-income countries' RPV viability.

Urbanization and climate change disproportionately affect worldwide rooftop solar viability for self-sufficient electricity

Jing Chen,[1] Yimin Chen,[1,*] Ming Luo,[1] Yuanzhi Yao,[2,*] Xiaocong Xu,[1] Weilin Liao,[1] Xiaoping Liu,[1,*] and Xia Li[2]

[1]School of Geography and Planning, and Guangdong Key Laboratory for Urbanization and Geo-simulation, Sun Yat-sen University, Guangzhou 510275, China

[2]School of Geographic Sciences, East China Normal University, Shanghai 200241, China

*Correspondence: chenym49@mail.sysu.edu.cn (Y.C.); yzyao@geo.ecnu.edu.cn (Y.Y.); liuxp3@mail.sysu.edu.cn (X.P.L.)

Received: October 15, 2025; Accepted: April 9, 2026; Published Online: April 17, 2026; https://doi.org/10.59717/j.xinn-geo.2026.100222

Citation: Chen J., Chen Y., Luo M., et al. (2026). Urbanization and climate change disproportionately affect worldwide rooftop solar viability for self-sufficient electricity. *The Innovation Geoscience* **4**:100222.

Rooftop photovoltaics (RPVs) play an increasingly critical role in global zero-carbon energy transition, yet underexplored is to what extent RPV potential can supply the ever-rising electricity demand under the combined effects of urbanization and climate change. Here, we project that the global RPV potential will grow by 13%—20% from 2015 to 2100 under four different socioeconomic-climate scenarios. This increase is primarily driven by RPV gains associated with urban expansion, although nearly one-fifth of them might be offset by climate-induced losses under high-emissions scenarios. However, future urban densification can drive down per capita RPV potential, which, alongside increasing individual consumption, will diminish RPVs' maximum feasible share in global electricity mix from 117% to 30%—47% by 2100. While simultaneously suffering from more severe and widespread high-emissions-induced losses, many developing countries, particularly the least developed, will undergo stronger urban densification, which shifts their RPV electricity supply-demand ratios from general surpluses over 200% to deficits much larger than those in wealthier countries. Given their reliance on RPVs for access to clean electricity, our results highlight the urgent need for strategic interventions, including embedding climate action into urban planning and accelerating global collaborative technological advancements, to mitigate these disproportionate impacts and foster an equitable energy transition.

INTRODUCTION

Ambitious climate mitigation targets aligned with the 2015 Paris Agreement require a global effort to accelerate the transition towards zero-carbon energy systems.[1] In this effort, rooftop photovoltaic (RPV) technology stands out as a vital solution because it can be deployed flexibly and rapidly, making it well-suited for supplying electricity in land-constrained urban environments and off-grid, impoverished regions.[2,3] The promotion of RPVs promises the co-benefits of reduced carbon emissions and universal electricity access,[4,5] thereby facilitating a more equitable energy transition. Propelled by cost reductions and policy incentives,[3] global RPV deployment has surged recently and is expected to be the fastest-growing electricity source in the coming decades.[6] As RPV penetration is likely to rise, accurate assessments of current and future global RPV technical potential (that is, the maximum achievable electricity generation given rooftop area, climatic conditions, and system performance)[7] are imperative for understanding the possible contribution of RPVs to electricity portfolios and informing decisions on policy-making.

RPVs represent a highly viable renewable electricity solution for dense urban areas by integrating into buildings without requiring additional land space,[7] which also means that the technical potential will change as urbanization proceeds. Urban expansion accompanied by increasing building stock leads to higher rooftop area, thus likely boosting RPV technical potential. However, urbanization is shifting toward more vertical development than lateral expansion,[8,9] suggesting more densely populated buildings that limit per capita access to RPV technical potential and challenge the feasibility of supplying sufficient electricity demand with RPVs. Beyond urbanization, inevitable climate change will further complicate the assessment of RPV technical potential. Specifically, RPV power output depends on downwelling shortwave radiation that determines solar resource availability, as well as other meteorological factors that affect panel efficiency, such as air temperature (higher temperatures typically reduce panel efficiency) and wind speed (moderate wind speed can provide panels with cooling).[10,11] Therefore, proper projections of RPV technical potential should account for the effects of both urbanization and climate change.

Previous research has investigated photovoltaic power output in a changing climate, revealing significant spatial and scenario variability in climate-induced impacts globally.[12-16] Their findings on climate-induced impacts are mixed, but in general, the impacts under low-emissions scenarios tend to be positive, while those under high-emissions scenarios tend to be negative. However, these studies concerned climatic conditions solely, excluding considerations of spatial availability primarily due to the challenges in obtaining high-quality estimates.[4] Recent efforts proposed that machine-learning-based methods offer the promise of large-scale and high-resolution rooftop area estimation that balances accuracy with computational efficiency,[3,4,17] but to date global maps of rooftop area and associated RPV technical potential are still limited. More importantly, the joint effects of urbanization and climate change on global RPV technical potential remain elusive. Considering the spatially heterogeneous nature of these two global changes, their consequences may differ across regions. This necessitates globally harmonized mapping to facilitate reliable cross-area comparisons, thereby providing a comprehensive global insight into future RPV technical potential changes and the attendant impacts on supply-demand relationships from an equitable and just energy transition perspective.

Here we assess the global effects of future urbanization and climate change on RPV technical potential alongside its maximum feasible share in the electricity mix, particularly focusing on regional differences. We employ the Shared Socioeconomic Pathways-Representative Concentration Pathways (SSP-RCP) framework to represent diverse futures for socioeconomic development and climate conditions.[18] At a high-resolution grid scale, we integrate machine-learning-based regression models and geospatial big data containing over 2 billion building footprints to project rooftop area and its growth accompanying urban expansion, and meanwhile utilize a physically-based photovoltaics performance model to simulate capacity factor (an indicator of electricity production from a generating unit)[19] under current and future climate conditions. Combining rooftop area with capacity factor, we generate RPV technical potential for the baseline year (2015) and at decadal intervals from 2020 to 2100 under four SSP-RCP scenarios, namely SSP1-2.6 (sustainability), SSP2-4.5 (middle of the road), SSP3-7.0 (regional rivalry), and SSP5-8.5 (fossil-fueled development). Further, we compare the assessed RPV technical potential with temporally aligned electricity demand data to explore its possible contribution to electricity supply. Our assessment is expected to improve the understanding of RPVs' potential role in energy transition, highlighting how uneven urbanization and climate change affect this role across countries with varying income levels.

MATERIALS AND METHODS

SSP-RCP scenario framework

We introduce a SSP-RCP scenario framework to explore possible futures under different socioeconomic narratives and global warming levels. This framework provides a foundation of assessments by the Intergovernmental Panel on Climate change,[20] and has been widely adopted in research regarding societal and climate futures.[21] The SSPs narrate alternative trends in socioeconomic development and environmental action, with each pathway distinguished by the quantified elements including population, urbanization, and GDP.[18] The RCPs, according to the target for end-of-century radiative forcing, represent diverse trajectories of greenhouse gas concentration related to energy system and land use.[22] Based on SSP-RCP integrated scenarios, we can derive the central characteristics of urbanization and climate change throughout the 21st century.

We consider four representative SSP-RCP scenarios, namely SSP1-2.6, SSP2-4.5, SSP3-7.0, and SSP5-8.5. Among them, SSP1-2.6 describes a sustainable pathway characterized by low emissions and mild climate change. It projects a world with low rates of urban land expansion and population growth, where global population will peak and then decline within the century. SSP2-4.5 is a middle-of-the-road pathway continuing along the historical development trend. In this scenario, global changes (including climate change caused by intermediate emissions, urban land expansion, and population growth) are considered to be moderate compared to other scenarios. SSP3-7.0 represents a regional rivalry pathway with high emissions resulting in moderate to severe climate change worldwide. Unlike the other three globalization scenarios, it assumes that countries focus on their domestic socioeconomic goals and develop independently, hence the rates of urban land expansion and population growth are low in industrialized countries but particularly high in developing countries. SSP5-8.5 assumes a fossil-fueled pathway facing a dramatic climate change due to the very high emissions. It yields a high rate of urban land expansion, but the population shows a low rate of growth, slightly higher than SSP1-2.6 while also showing a peak-to-decline trend.

Datasets

Building footprint data. We utilize three open datasets of building footprints to generate the baseline year (2015) rooftop area. Specifically, the building footprints from Google Open Buildings are used for the entire African continent and Southeast Asia,[23] while the building footprints produced by Microsoft are used for most of the remaining regions.[24] For China, however, its building footprints are not available in these two datasets. Therefore, we use another open dataset of building footprints in China as a complement.[25] By using all these datasets, we aggregate the building footprint area at the 3 km × 3 km grid level, and the results are regarded as the ground truth rooftop area for the baseline year under the assumption that building footprint area can approximate rooftop area.

Data for generating the predictors of rooftop area extrapolation models (REMs). The data used for generating the predictors of REMs includes urban land maps, gridded population, road network, digital elevation model (DEM), and climate zone classification. The urban land maps are acquired from ref.[26], which includes a 2015 urban land map and the projected urban land maps from 2015 to 2100 at 10-year interval under the four selected SSP scenarios. The gridded population data in 2015 are obtained from WorldPop,[27] while the SSP projections of population distribution spanning from 2020 to 2100 at 10-year interval are obtained from ref.[28] The road network data are acquired from ref.[29], which provides five functional groups of roads (i.e., local, tertiary, secondary, primary, and highway). The DEM data are obtained from the National Oceanic and Atmospheric Administration of the United States,[30] based on which the data of slope are generated. Finally, the map of Köppen-Geiger climate zone classification is also collected.[31] All these data, excluding the road network data in vector format, consistently have a spatial resolution of 1 km.

Climate scenario data. The meteorological variables (irradiance, temperature, and wind speed) under different scenarios are obtained from the NASA Earth Exchange Global Daily Downscaled Projections (NEX-GDDP-CMIP6),[32] which provides the daily-level bias-corrected climate change projections with a spatial resolution of 0.25°. Considering the availability of the required variables for projecting RPV potential, climate projections made from 13 models of NEX-GDDP-CMIP6 (Table S1) are used to account for the uncertainty caused by using a single model. Note that the projection under SSP2-4.5 in 2015 is treated as historical climate conditions at the baseline year.

Photovoltaic technical data and electricity demand data. The photovoltaic technical data, including optimal tilt angle and module parameters, are applied for capacity factor assessments. The mapping of optimal tilt angle for maximizing the annual photovoltaic generation is generated by the Global Solar Atlas.[33] We use the maximum value of the dataset (50°) as the optimal tilt angle for regions above 60°N where angle values are absent. The module parameters required to model photovoltaic systems are retrieved from the California Energy Commission photovoltaic module database.[34] Furthermore, the national-level electricity demand for the baseline year and the SSP scenarios is obtained from ref.[35]

Mapping of rooftop area

We refer to a machine-learning-based framework that combines both top-down and bottom-up approaches to estimate rooftop area at a resolution of 3 km.[3,4,17] The top-down approach applies high-resolution spatial techniques like Light Detection and Ranging or machine-learning-based object detection to obtain vectorized rooftop area, which is then quantified at the grid scale. Here we achieve this by aggregating vector building footprints with global coverage (see Datasets section). The bottom-up approach takes the obtained gridded rooftop area as a sample to model its relationship with various geospatial variables, and then uses the modeled relationship to extrapolate rooftop area to regions outside the sample. We establish REMs to perform rooftop area extrapolation. By utilizing multi-temporal geospatial variables, we conduct the extrapolations for global rooftop area in the baseline year as well as for future rooftop area growth under different scenarios.

REMs. The machine learning method of Gradient Boosting Decision Trees (GBDT) is used to develop REMs. Specifically, three representative GBDT algorithms, namely XGBoost,[36] CatBoost,[37] and LightGBM,[38] are used to perform regression between rooftop area and a set of predictors at the 3 km grid level. The training is implemented by using the Python packages of *xgboost*, *catboost*, *lightgbm*, *category-encoders*, *bayesian-optimization*, and *scikit-learn*.

By using the geospatial data mentioned in the *Datasets* section, a set of predictors are generated for the REMs. These include the sum of urban land area and population within each 3 km grid and the corresponding neighborhood statistics of sum, maximum, and variance. The neighborhood sizes include 3 × 3, 5 × 5, and 7 × 7. Additionally, the total road length and the corresponding lengths for each of the five road types are calculated for the 3 km grids. The values of elevation and slope are aggregated to the 3 km grids through averaging. The climate zone classification is resampled to 3 km applying the rule-of-majority. The full list of these predictors can be found in Table S2.

We develop 30 region-specific REMs. In each of the 30 macro regions modified from the SSPs database (Figure S1), the sample of rooftop area is randomly split into the training set and the testing set (75% and 25%, respectively). The training set is used for hyperparameter tuning and model training, while the testing set is used for evaluation. Hyperparameter tuning is implemented by using Bayesian optimization and the 5-fold cross-validation approach. Five hyperparameters are tuned: the number of iterations that specifies the number of trees; the maximum depth and minimum sample size that control the tree complexity; the learning rate and the L2 regularization that determine the fitting performance. More details of the tuning results are given in Table S3. After training, for a certain region, the performances of the three fine-tuned GBDT models are evaluated with the testing set, and the best one is used to project the rooftop area for that region.

The evaluation of REMs demonstrates a global R^2 of 0.84, with regional R^2 ranging from 0.64 to 0.92 (Figure S2). The per grid mean absolute error and root mean square error are 0.17 and 0.25 km^2, respectively, with the highest values observed in India (0.30 and 0.43 km^2, respectively). The relative error between the prediction and the observation is 0.04%.

To further assess REMs' reliability and robustness, we construct supplemental models for performance comparison. Since the validity of using random train-test splits for validating model's generalization ability, though it has long been proven, may be challenged because the spatial autocorrelation could lead to optimistically biased estimates,[39] we present the prediction error when using spatially blocked splits for model building (Figure S17; see Text S1 for detailed methodologies). The result shows a distribution generally similar to the error observed in REMs, justifying our generalization evaluation. Additionally, while previous studies often used a single global model to predict rooftop area,[3,17] our comparison between the REMs and the global model developed using the same procedures shows that using REMs would yield better predictions in most regions (Figure S2).

Rooftop area extrapolations. We first extrapolate the rooftop area sample aggregated from building footprints to out-of-sample grids using REMs. In particular, we obtain a globally seamless rooftop area map for the baseline year of 2015, and then conduct the scenario extrapolations for future rooftop area growth based on this baseline map. The scenario extrapolations are made per decade from 2020 to 2100. For each time episode (year) to be predicted, we implement the REMs for grids that have increased urban land area compared to the previous time point. When applying the REMs, the predictors of urban land area and its neighborhood statistics, as well as population and its neighborhood statistics, are updated using the projections obtained from ref.[26] and ref.[28], respectively, while the values of the other predictors (road length metrics, slope, elevation, and climate zone classification) remain unchanged. This could be one limitation of our method, mainly owing to the lack of scenario projections of road network and climate zone classification. For the terrain conditions, it is somehow reasonable to assume they remain constant by the end of this century. According to our assessment of variable importance in REMs, predictors associated with urban land area and population collectively contribute over 70% of the overall importance (Figure S19; see Text S2, Figures S18 & S20 for more discussion). This supports our assumption that these time-varying predictors reasonably capture the dynamics of rooftop area.

In this study, building footprint is taken as the simplified representation of roof geometry, with its area serving as a proxy for rooftop area. This may introduce some discrepancies as the real-world roofs are diverse in shapes. For instance, residential buildings often feature flat roofs that can be directly mapped by building footprints, or alternatively feature shed and gable roofs that have slightly larger rooftop surfaces. Mixed-use buildings, however, commonly exhibit complex-shaped roofs, resulting in reduced rooftop area relative to building footprints.[40] To date, accurate estimation of footprint-to-rooftop ratio remains a complex task, with few studies providing comprehensive information for large-scale applications. Given this limitation, we assume building footprint area to be rooftop area in reference to previous studies.[3,4]

We note that our extrapolations aim to contextualize the changes in rooftop area within the socioeconomic development under different scenarios. The extrapolation scheme presumes the spatiotemporal representativeness of REMs while not accounting for the complex processes (e.g., urban planning) that may affect the long-term dynamics. The value of this approach lies primarily in its descriptive strengths rather than its predictive capabilities. We acknowledge that efforts like incorporating domain-specific knowledge could improve the extrapolations, but such detailed analysis is beyond the scope of this study. Nonetheless, the socioeconomic narratives underlying each scenario can be viewed as a proxy for urban planning paradigms, hence our scenario projections are able to provide a forward-looking insight into how rooftop area might change under these paradigms.

Capacity factor assessment

Capacity factor is calculated as the ratio of the actual annual electricity generation to the maximum possible generation if the photovoltaic device operated at nameplate capacity throughout the year. With the open-source PVLIB-Python library,[41] the capacity factor at 3 km resolution is generated in a grid-by-grid manner following three steps:

(1) System configuration: the power system, fixed at the optimal tilt angle (determined using data from Global Solar Atlas,[33] see Datasets section) with a south-facing/north-facing orientation in the Northern/Southern Hemisphere, consists of the modules to convert sunlight into direct current (DC) and the inverters to transform DC to alternating current (AC). We assume the system uniformly utilizes module with a conversion efficiency of 19.6% (nameplate capacity of 350 W) and inverter with a designed efficiency of 96.5%. Detailed technical parameters are listed in Table S4.

(2) Plane-of-array irradiance modelling: the plane-of-array irradiance, or the actual solar radiation collected by the system for electricity generation, comes from three sources, i.e., direct beam, sky diffuse, and ground-reflected irradiance. Each of the sources is calculated based on the direct normal irradiance (*DNI*, W m^{-2}), the diffuse horizontal irradiance (*DHI*, W m^{-2}), and the global horizontal irradiance (*GHI*, W m^{-2}). Given that plane-of-array irradiance modelling requires hourly *DNI*, *DHI*, and *GHI* inputs, but only daily mean *GHI* is available in NEX-GDDP-CMIP6 climate projections, we adopt an artificial diurnal cycle following a sinusoidal function to downscale *GHI* into hourly resolution,[42] and then utilize the DIRINT decomposition model to obtain *DNI* from *GHI*,[43] and calculate *DHI* as follows:

$$DHI = GHI - (DNI \times \cos(\theta_Z)) \tag{1}$$

where θ_Z is the solar zenith angle (degrees), estimated via NREL solar position algorithm considering geographic position (longitude, latitude, and altitude) and the hour of the day.[44]

The sky diffuse (I_d, W m^{-2}) is transposed from *DHI* using Hay/Davies transposition model,[45] while the direct beam (I_b, W m^{-2}) incident on the plane and ground-reflected irradiance (I_g, W m^{-2}) can be calculated with straightforward geometry as follows:

$$I_b = DNI \times \cos(AOI) \tag{2}$$

$$I_g = GHI \times albedo \times \frac{(1 - \cos(\theta_T))}{2} \tag{3}$$

$$AOI = \cos^{-1}(\cos(\theta_Z) \times \cos(\theta_T) + \sin(\theta_Z) \times \sin(\theta_T) \times \cos(\theta_A - \theta_O)) \tag{4}$$

where *AOI* is the angle of incidence (degrees), determined by system morphology (tilt angle θ_T, degrees; orientation θ_O, degrees) and solar position (θ_Z; azimuth angle θ_A, degrees). The *albedo* value is set using the default one (0.18) assigned by PVLIB for urban surface. Finally, the plane-of-array irradiance (I_{tot}, W m^{-2}) is obtained by summing up irradiance from the three sources:

$$I_{tot} = I_b + I_d + I_g \tag{5}$$

(3) Radiation-electricity conversion and capacity factor calculation: The available solar radiation depends on I_{tot}, while the radiation-electricity conversion is affected by module temperature. On a daily basis, we feed the I_{tot} (24 hourly values per day), along with temperature and wind speed that influence the module temperature (for these two factors, the daily averages can be used without significant error),[42] into the Sandia Photovoltaic Array Performance Model to estimate the electricity generation.[46] The capacity factor (*CF*, a unitless ratio) is then calculated as follows:

$$CF = \frac{E_{annual}}{C_{module} \times 8760} \tag{6}$$

where E_{annual} is the electricity generation aggregated from daily values to an annual total (Wh), C_{module} is the nameplate capacity of module (350 W), and the number 8760 refers to the total hours in a year.

Here we employ a technically rigorous approach to improve the reliability of electricity generation assessments compared to previous global-scale studies,[3,12,13,17] but we also incorporate some assumptions to handle the complexities in long-term assessment. For instance, we do not consider the lifetime degradation of RPVs as this relies on where and when the RPVs are deployed. We assume that installed RPVs receive adequate cleaning and maintenance during operation so that soiling or failure can be ignored, while in reality this depends on natural precipitation as well as labor and economic investments. We set unified technical components globally, but affluent households can achieve higher RPV potential by adopting cutting-edge technologies such as sun-tracking systems. In addition, considering the long time span of our study during which significant technological progress (primarily in module technology)[47] is expected, we supplement two sets of experiments using advanced modules with conversion efficiencies of 25.8% (436 W) and 31.1% (526 W). The conversion efficiency of the three modules we selected reflects the current technical level, recent record, and theoretical limit of silicon-based modules that dominate the market.[48] Experimental results are presented in Table S5 to better understand how technological advancements may affect our main results.

RPV potential calculation

Combining the values of rooftop area (A_{roof}, m^2) and capacity factor (*CF*), we can obtain the RPV potential (*P*, Wh) for each 3 km resolution grid through the following calculation:

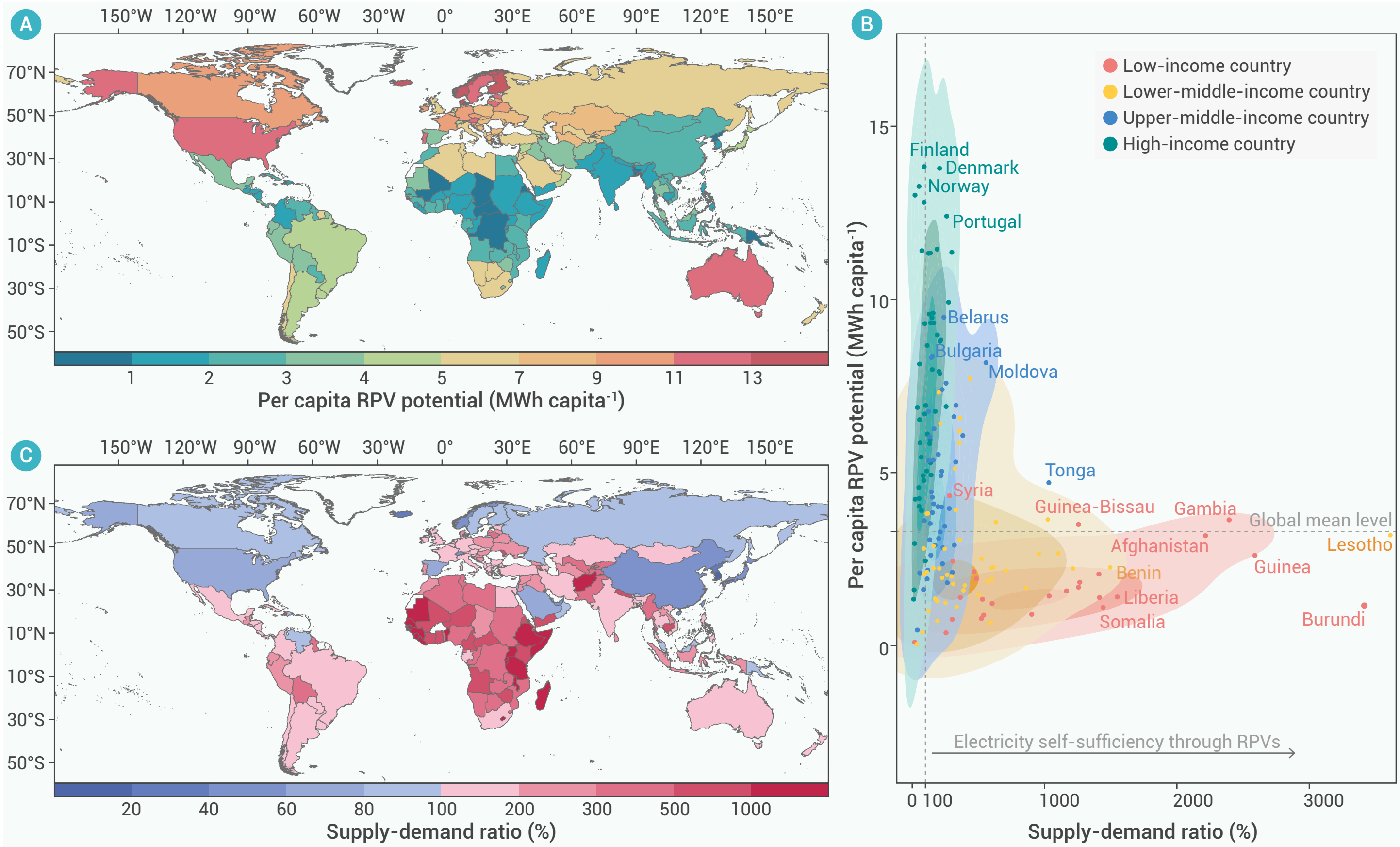

Figure 1. Global patterns of per capita RPV potential and the supply-demand ratio of RPV electricity in 2015 (A) Per capita RPV potential in 2015 at the national scale. (B) Uneven distribution of per capita RPV potential and supply-demand ratio across the income level. The dots represent country-level estimates of per capita RPV potential and supply-demand ratio, and the shadings display the kernel density distribution of the dots grouped by income level. The income classification follows that of the World Bank (see Figure S3 for details). (C) Supply-demand ratio in 2015 at the national scale.

$$P = A_{roof} \times RAF \times \frac{C_{module}}{A_{module}} \times 8760 \quad \times CF \quad (7)$$

where *RAF* is the rooftop availability factor (the ratio of available rooftop area for RPV installation to the total rooftop area), while C_{module} and A_{module} are the nameplate capacity (350 W) and size (1.79 m^2) of the module, respectively.

The rooftop availability factor is a commonly used measure in large-scale RPV research, indicating the loss of rooftop area because of geographic constraints such as roof morphology, obstacles, and shading effects. Here we use a rooftop availability factor of 0.32 for the main results according to the general cases reported (Table S6). This is a trade-off in the absence of comprehensive region-specific references globally. As the rooftop availability factor may vary regionally, we provide a series of regional RPV potential assessments using varying rooftop availability factors to explore the possible impact (Tables S7 & S11). Given that some countries have started reserving rooftop space for RPV installation in the building design process,[49] rooftop availability factor may increase and likely converge globally as more countries adopt this practice.

RESULTS

Achievable electricity self-sufficiency through RPVs in the baseline year (2015)

We estimate that the global annual RPV technical potential (hereafter RPV potential) for the 2015 baseline year is 23.9 PWh, equivalent to 3.3 MWh per capita. However, per capita RPV potential varies significantly across different income-group countries (Figures 1A-B). Among the four income groups, per capita RPV potential in high-income group is 8.3 MWh, which is more than double that in upper-middle-income group (3.1 MWh) and even four times that of lower-middle- and low-income groups (1.5 MWh and 2.1 MWh, respectively). Countries with above-the-global-mean per capita RPV potential are mostly high- and upper-middle-income countries (representing 51% and 34%, respectively), while lower-middle- and low-income countries collectively account for only 15% (Figure 1B). All countries with per capita RPV potential greater than 10 MWh belong to high-income group, while among the 26 low-income countries, only Syria, Gambia, and Guinea-Bissau barely reach the global mean level.

The dominance of developed countries in per capita RPV potential is primarily due to their large built-up areas and relatively small populations, which result in a higher per capita building stock available for RPV installation. Some emerging countries also have considerable built-up areas but are densely populated, leading to less per capita building stock and hence lower per capita RPV potential. For instance, despite ranking among the top ten countries in total RPV potential (over 0.5 PWh, detailed in Figure S4), the per capita RPV potentials in China (2.1 MWh), India (1.0 MWh), Brazil (4.3 MWh), Indonesia (2.4 MWh), and Mexico (3.8 MWh) are similar to, or even below, the global mean. Other developing countries, especially those in Africa, generally have abundant solar resources and hence higher RPV generation per unit area (Figure S5), yet limited building stock constrains their current RPV potential.

Despite the uneven distribution of RPV potential, more than 80% of countries worldwide can achieve self-sufficiency in electricity by fully exploiting their RPV potential. Nonetheless, the ratio of potential RPV electricity production to total electricity demand (hereafter, the supply-demand ratio) still varies evidently across countries and income levels (Figures 1B-C), showing an almost opposite pattern to per capita RPV potential. That is, economically underdeveloped countries tend to have higher supply-demand ratios than the developed. Countries with a supply-demand ratio below 100% are mainly developed economies in the Northern Hemisphere (excluding most European countries), along with a few developing countries such as China, Venezuela, and Malaysia. This contrasts with Africa, where most countries have a supply-demand ratio of over 200%, with some even reaching 1000% (e.g., Lesotho, Burundi, Guinea). Overall, if the current RPV potential can be fully leveraged to generate electricity, it would cover 116.7% of the world's electricity demand in

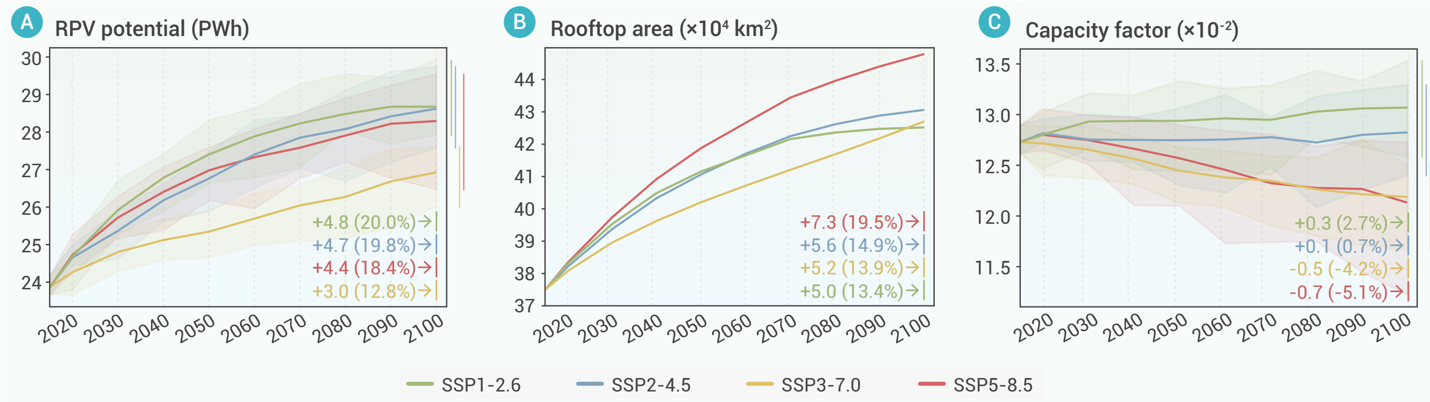

Figure 2. Projected RPV potential under different future scenarios of urban expansion and climate change (A) Growth in global RPV potential from 2015 to 2100 under four SSP-RCP scenarios. The growth rates of RPV potential from 2015 to 2100 are provided in the lower right corner. The shaded areas represent the inter-model spread of the 13 CMIP6 models (Table S1). (B & C) Similar to (A), but for the growth of rooftop area resulting from urban expansion and change in capacity factor due to climate change, respectively.

2015. It should be noted that the supply-demand ratio is based on technical potential, implying that realization of this theoretical maximum remains constrained by factors such as storage efficiency, grid stability, and transmission losses, which are beyond the scope of our analysis.

The primary reason for the opposite distribution pattern between per capita RPV potential and supply-demand ratio is that electricity demand typically rises with income. For example, in 2015, the total electricity demand in low-income countries combined (119 TWh) is a negligible 3% of that in the United States (4151 TWh), while in lower-middle-income countries (2241 TWh) it is 54% of the United States' level. Therefore, many developed countries, even with higher per capita RPV potential, cannot achieve electricity self-sufficiency through RPVs alone. By contrast, low- and lower-middle-income countries may even have considerable surplus RPV electricity to be stored or transmitted elsewhere.

Total RPV potential regarding urban expansion and climate change

Global RPV potential is expected to increase from 2015 to 2100 under all four assessed scenarios (Figure 2A). The three scenarios in the context of global cooperation exhibit similar trends, but as the assumed greenhouse gas emission rises, the growth rate (2015-2100) of global RPV potential declines (i.e., 20.0%, 19.8%, and 18.4% under SSP1-2.6, SSP2-4.5, and SSP5-8.5, respectively). The SSP3-7.0 scenario (uniquely marked by regional rivalry) yields the lowest growth rate of 12.8%, significantly lagging behind the other scenarios.

The growth of RPV potential is primarily driven by the increased rooftop area resulting from urban expansion, while the impact of climate-induced changes on capacity factor cannot be overlooked (Figures 2B-C & 3). The rooftop area is projected to continue expanding during 2015-2100 across all scenarios (Figure 2B). By 2100, global rooftop area is projected to expand by 19.5% under SSP5-8.5 and by 13.4-14.9% under other scenarios. Considering only rooftop expansion, global RPV potential will rise by 16.1% under SSP1-2.6, 17.5% under SSP2-4.5, 16.6% under SSP3-7.0, and 24.0% under SSP5-8.5. Capacity factor, however, is affected by climate change in different ways and to varying degrees across scenarios (Figure 2C, see Text S3 for further discussion on the variation of meteorological variables and their impact on capacity factor). From 2015 to 2100, low-emissions SSP1-2.6 will see an increase of 2.7% in global mean capacity factor, which can individually boost global RPV potential by 3.4%. Under intermediate-emissions SSP2-4.5, global mean capacity factor tends to remain stable, with a 0.7% increase by 2100 which contributes to a 2.0% growth in global RPV potential. Under high-emissions SSP3-7.0 and SSP5-8.5, climate change will diminish global mean capacity factor by 4.2% and 5.1%, respectively, corresponding to losses of 3.0% and 4.4% in global RPV potential. This negative impact of climate change explains why SSP5-8.5 (despite having a much larger increase in rooftop area) exhibits a lower growth of global RPV potential than SSP1-2.6 and SSP2-4.5. Although rooftop expansion dominates the changing magnitude of global RPV potential, it spans exclusively a small geographic extent (the grids with rooftop expansion account for less than 4% of the total grids across all scenarios; see Figures S6-S7). By contrast, the climate change impacts are distributed on a wider scale globally, with the proportion of negatively affected grids being 19%, 44%, and over 85% under low-, intermediate-, and high-emissions scenarios, respectively (Figure S8).

Driven by the combined effects of spatially heterogeneous rooftop expansion and climate change, our projections reveal regional variations in RPV potential growth (Figure 3). Low- and lower-middle-income groups of countries stand out for their rapid rooftop expansion and hence significantly higher RPV potential growth rates (> 25%) under SSP1-2.6, SSP2-4.5, and SSP3-7.0. Under SSP5-8.5, the highest growth rate of 23% appears in high-income group, which will experience rooftop expansion of similar magnitude as low- and lower-middle-income groups under the same scenario. Notably, climate change exerts distinct influences on different income-group countries. In low-income group, only under SSP1-2.6 does future climate change positively affect RPV potential, inducing the smallest gains of 1.7% across the groups. However, low-income group suffers the most from high emissions with climate-change-induced losses of 7.6% under SSP3-7.0 and 7.2% under SSP5-8.5, which will offset 23% and 30% of the gains from rooftop expansion, respectively. In lower-middle-income group, RPV potential benefits more from climate change under SSP1-2.6 and SSP2-4.5 (with respective gains of 4.9% and 2.0%), but is also significantly harmed under SSP3-7.0 and SSP5-8.5 (with respective losses of 6.4% and 3.0%, offsetting 18% and 14% of rooftop-expansion-driven gains). By contrast, high-income group shows relatively modest responses to climate change across scenarios, while upper-middle-income group not only have the strongest resilience to negative impacts of high emissions but also reap the greatest benefits under low- and intermediate-emissions scenarios. In upper-middle-income group, the gains from climate change contribute substantially to RPV potential growth, equivalent to 101% (SSP1-2.6) and 53% (SSP2-4.5) of those derived from rooftop expansion.

At the country level, growth rates of RPV potential in 38 countries in South Asia, West Asia, and sub-Saharan Africa (28 of which are low- and lower-middle-income countries) surpass the global mean across scenarios (Figure S9). However, under high-emissions scenarios, several countries (primarily developed countries under SSP3-7.0 and developing countries under SSP5-8.5) will face reduced RPV potential since climate-change-induced losses outweigh rooftop-expansion-driven gains. Among the 26 low-income countries, climate change impacts will offset over 20% of the gains from rooftop expansion in 15 countries under SSP3-7.0 and 18 under SSP5-8.5 (Table S8). This offset rate exceeds 50% in Ethiopia, Yemen, Rwanda, Afghanistan, and Guinea-Bissau.

Per capita RPV potential in the context of urban densification

Increasing population accompanied by urban densification can dilute the growth of RPV potential on a per capita basis. Regardless of scenarios, projections for 2015-2100 reveal a worldwide trend of urban densification. This increase in urban density (measured as population per m^2 of rooftop area) is expected in at least 60% of countries (Figure S10). Globally, mean

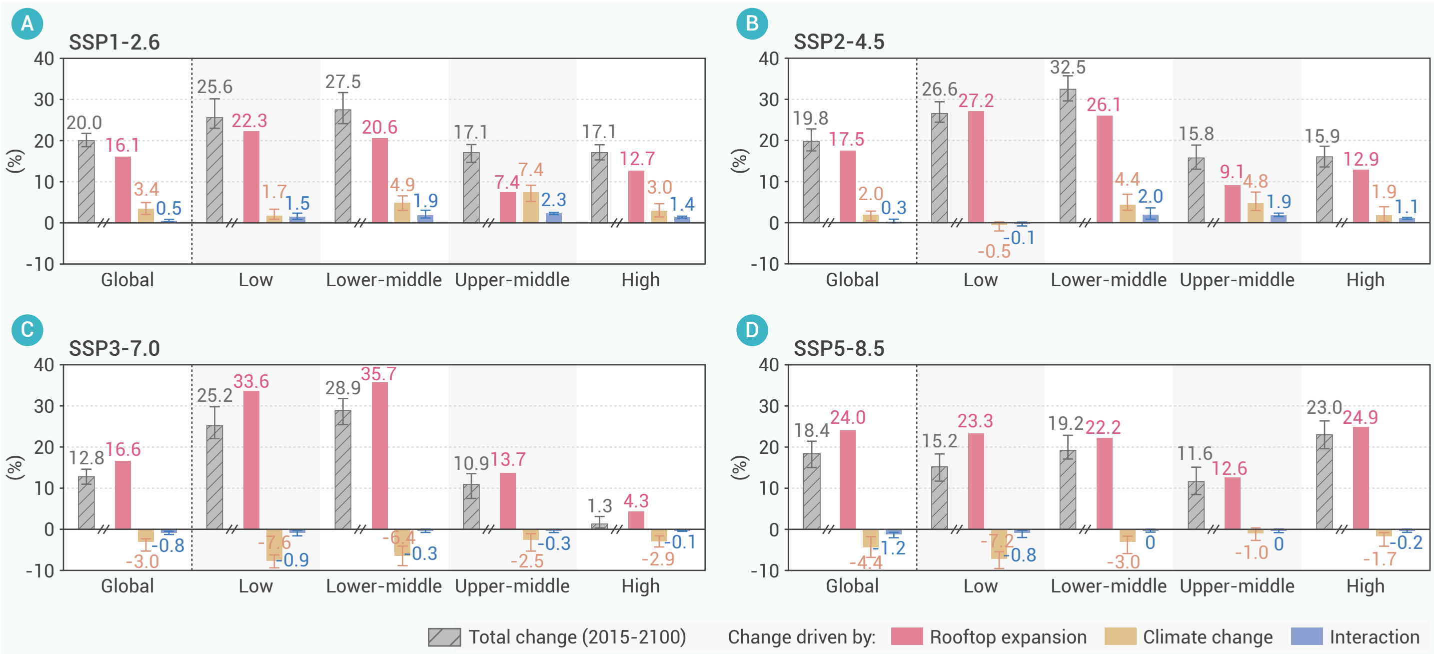

Figure 3. Contribution of rooftop expansion, climate change, and their interaction to RPV potential changes from 2015 to 2100 Contribution to RPV potential changes under SSP1-2.6 (A), SSP2-4.5 (B), SSP3-7.0 (C), and SSP5-8.5 (D) at the global and regional levels. Error bars represent the inter-model spread of the 13 CMIP6 models. The contributions of rooftop expansion and climate change are isolated by fixing one of the two factors (rooftop area and capacity factor) at the 2015 level while allowing the other to vary toward the 2100 level when calculating RPV potential. The remaining RPV potential change not explained by rooftop expansion and climate change is attributed to the interaction of these two factors.

urban density can peak at 1.3-2.1 times the baseline level across scenarios, with SSP1-2.6, SSP5-8.5, SSP2-4.5, and SSP3-7.0 ranked in ascending order of magnitude (Figure S11). Even under the scenarios where global population will decrease after mid-century, global mean urban density only sees a minimal decline from its peak value. This trend towards densification presumably drive RPV potential to grow slower than population, contributing to the inverse correlation between population size (Figure S11) and per capita RPV potential (Figure 4A). Under SSP1-2.6 and SSP5-8.5, per capita RPV potential at the global scale will decline slightly before rebounding and subsequently exceeding the baseline level in the 2050s and 2070s, respectively. Their rebound will lead to an increase in rates of 26.4% under SSP1-2.6 and 16.6% under SSP5-8.5 in 2100 relative to 2015. Under SSP2-4.5, global per capita RPV potential is anticipated to follow a U-shaped trajectory, dropping 11% in 2050 and ending 3.5% below the baseline in 2100. The strongest reduction of 35.5% occurs under SSP3-7.0, where global per capita RPV potential will decrease monotonically.

The marked regional disparity that higher-income countries tend to have greater per capita RPV potential is expected to persist in the future. Under all scenarios, low-income group of countries will experience the steepest decline in per capita RPV potential, eventually displacing lower-middle-income group as the lowest-ranked after mid-century (Figure S12). While rapid urbanization in low-income countries will considerably increase RPV potential through urban land expansion, it will in turn lower per capita level as a result of densification and fast-growing population. The expected reductions are 25.2%, 49.0%, 66.8%, and 28.8% under SSP1-2.6, SSP2-4.5, SSP3-7.0, and SSP5-8.5, respectively (Figure 4B). Even under its most optimistic scenario SSP1-2.6, the percentage reduction for low-income group is greater than that for either upper-middle- or high-income groups under their most pessimistic scenarios. By contrast, upper-middle-income group will consistently exhibit the strongest increases in per capita RPV potential compared to other groups (except under SSP3-7.0, which predicts a slight decline), nearly doubling under SSP1-2.6 and SSP5-8.5. Nonetheless, high-income group maintains the greatest per capita RPV potential over the century.

Low- and lower-middle-income countries constitute the majority of 35 countries that are projected to face decreased per capita RPV potential under all scenarios (Figure 5). Notably, 14 of these countries show above-the-global-mean growth rates of RPV potential. A representative example is Mali in Africa, where the national total RPV potential is expected to rise by 56%-89%, yet the per capita potential will decline by 6.4%-50.7%. In comparison, 32 countries show increased per capita RPV potential across scenarios, and most of them have high- and upper-middle-income levels, spatially clustered in East Asia (e.g., 39%-173% increases in China, 32%-173% in Japan, and 37%-158% in South Korea), the Middle East (e.g., 34%-105% in Iran and 65-77% Lebanon), and Europe (e.g., 7%-130% in Germany, 13-96% in Italy, and 3%-72% in Spain).

Feasibility of RPVs for supplying future electricity demand

Looking to 2100, global electricity demand is projected to grow by 2.8-4.6 folds, mainly attributed to low- and lower-middle-income countries (Figure S13). At per capita level, there will also be continuous increases across the countries (Figure 6). Nevertheless, convergence in per capita electricity demand between low-/lower-middle-income and upper-middle-/high-income countries is expected exclusively under the scenarios featuring rapid electrification (SSP1-2.6 and SSP5-8.5).[50] Under scenarios of moderate (SSP2-4.5) and slow (SSP3-7.0) electrification, per capita electricity demand in low- and lower-middle-income countries, albeit with much higher relative growth, is likely to remain far less than in upper-middle- and high-income countries throughout the century.

Rapid demand-side growth, coupled with diminishing per capita RPV potential supply under most scenarios (Figure 4B), results in the dramatic decreases in supply-demand ratio in low- and lower-middle-income groups of countries (Figure 6). Supply-demand ratio in low-income group will fall below that of upper-middle- and high-income groups around the 2060s, while lower-middle-income group appears to progress faster, becoming the group with the lowest supply-demand ratio from the 2030s onward. This plummeting supply-demand ratio means that RPVs' maximum feasible share in the electricity mix of low- and lower-middle-income groups might drop from a baseline of tremendous surplus to less than 20% by 2100 (except under SSP3-7.0). As regards upper-middle- and high-income groups, the supply-demand ratio, which roughly meets self-sufficiency in the baseline year, will also face an anticipated decline though to a smaller extent. In 2100, the supply-demand ratio in upper-middle-income group will decline to 38%-48%, while in high-income group it will range from 47% to 71% under the globalization scenarios (i.e., SSP1-2.6, SSP2-4.5, and SSP5-8.5) and remain almost unaffected at 96% under SSP3-7.0. By the century's end, the supply-demand ratio distribution may invert compared to the 2015 baseline, that is,

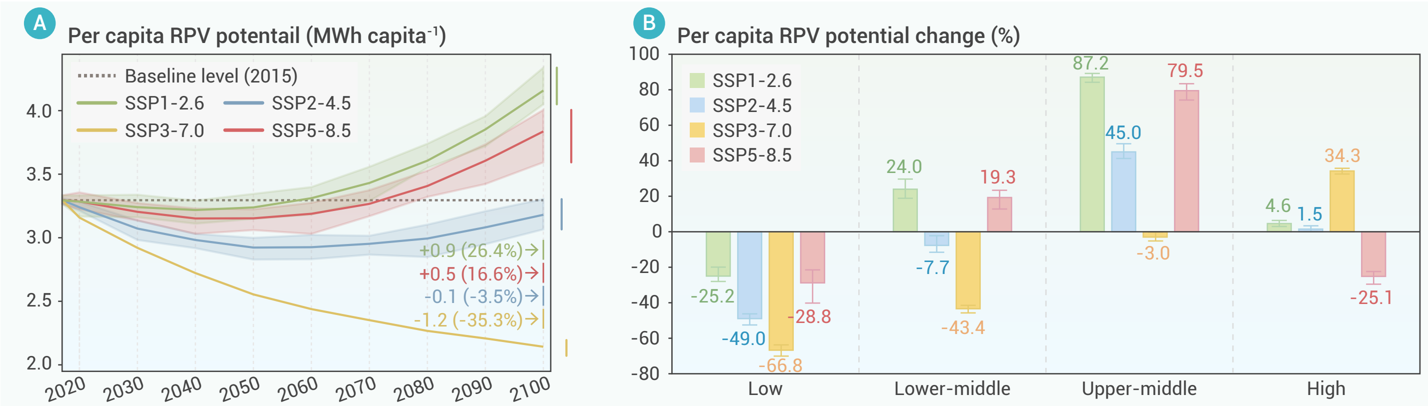

Figure 4. Projected per capita RPV potential from 2015 to 2100 (A) Change in global per capita RPV potential from 2015 to 2100 under four SSP-RCP scenarios. The change rates of per capita RPV potential between 2015 and 2100 are provided in the lower right corner. The shaded areas represent the inter-model spread of the 13 CMIP6 models (Table S1). (B) Change rates of per capita RPV potential between 2015 and 2100 at the regional level. Error bars represent the inter-model spread of the 13 CMIP6 models.

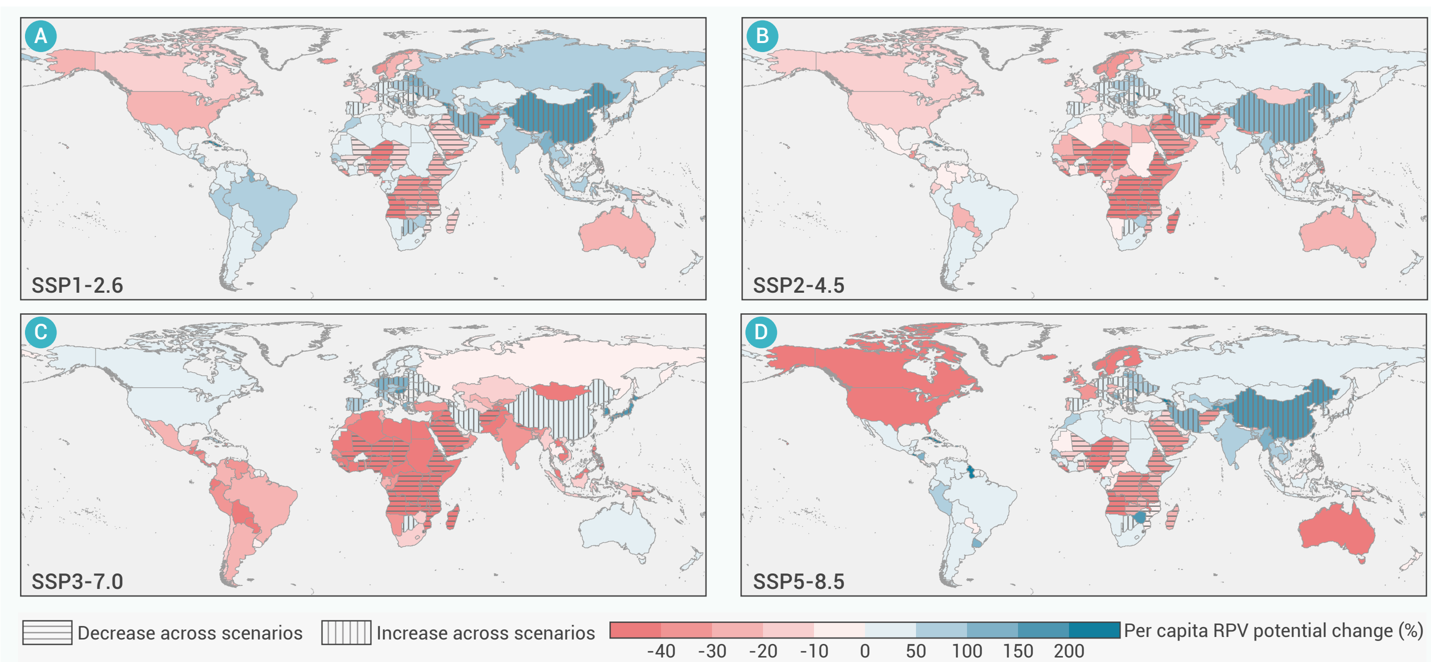

Figure 5. Spatial distribution of projected change in per capita RPV potential Change rate of country-level per capita RPV potential between 2015 and 2100 under SSP1-2.6 (A), SSP2-4.5 (B), SSP3-7.0 (C), and SSP5-8.5 (D). The countries with consistently increasing or decreasing per capita RPV potential across scenarios are highlighted with shade.

developed countries tend to have higher ratios than the underdeveloped.

Though universally deteriorating supply-demand ratios may hinder the feasibility of deploying RPVs to ensure future electricity self-sufficiency, fully utilized RPV potential would still be adequate for supplying 30%-47% of the global demand in 2100. Noteworthy here is the supply-side contribution in counterbalancing the rising demand, such that SSP1-2.6 (with larger demand) yields a higher supply-demand ratio than SSP2-4.5 due to stronger supply-side gains. This contribution is more pronounced when comparing the supply-demand ratio in upper-middle-income group across different scenarios. In upper-middle-income group, compared to SSP3-7.0 which in per capita terms predicts the lowest demand growth but lightly diminished supply by 2100, the other scenarios with prominent per capita RPV potential gains could achieve higher supply-demand ratios. Better still, supply-side gains outstrip demand-side growth in several countries, thus increasing their supply-demand ratios (Figure 7). This mainly occurs in high-income countries under SSP3-7.0, with Japan and South Korea showing such an increase under all scenarios except SSP5-8.5. Moreover, there are still a few countries possessing sufficient RPV potential to completely satisfy their electricity demand during the century (Figure S14). For instance, Bulgaria, Belarus, Bosnia and Herzegovina, Croatia, Latvia, and Lithuania in eastern Europe can achieve electricity self-sufficiency through RPVs irrespective of scenarios, while some of the other European countries can also do that under most scenarios.

DISCUSSION

Comparison results with previous studies

To incorporate the effects of urban expansion and climate change into RPV potential projections, we generate high-resolution global maps of rooftop area, capacity factor, and resulting RPV potential under four SSP-RCP scenarios spanning 2015 to 2100. This work, to our knowledge, is the first attempt to take these two global changes into account to project the spatially explicit RPV potential with global coverage under SSP-RCP framework, allowing direct comparisons with existing literature only for the baseline year. At the global level, our estimated RPV potential (23.9 PWh) falls between the two recent grid-level studies (19.5 PWh and 27 PWh).[3,17] The discrepancies originate largely from estimated rooftop area and methods for assessing photovoltaic generation. Regarding rooftop area estimation, ref.[3] used a sample of 0.3 billion buildings that is heavily biased towards developed regions, potentially causing uneven estimation quality. Ref.[17] mitigated such bias errors through stratified sampling from representative regions, but its sample size is relatively small and the rooftop area is considered underestimated.[17] Our study assembles a more spatially comprehensive sample that includes over

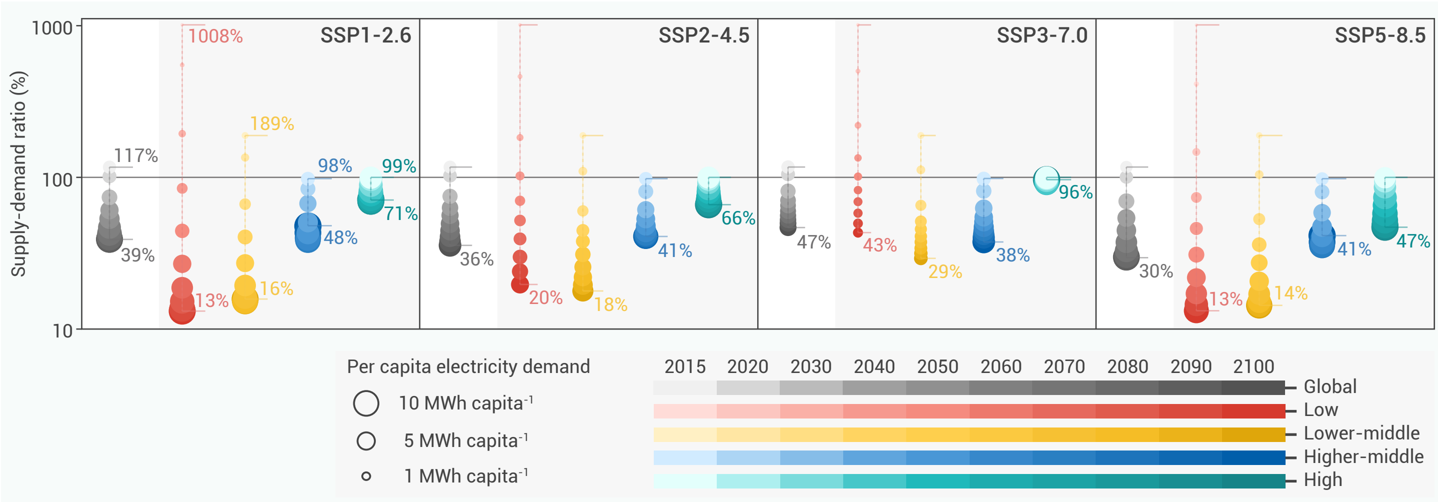

Figure 6. Projected supply-demand ratio for RPV electricity from 2015 to 2100 Global and regional supply-demand ratios from 2015 to 2100 under four SSP-RCP scenarios. Size of the circle represents per capita electricity demand, and color indicates the year as well as the region categorized by income level. The supply-demand ratios for 2015 and 2100 are labelled.

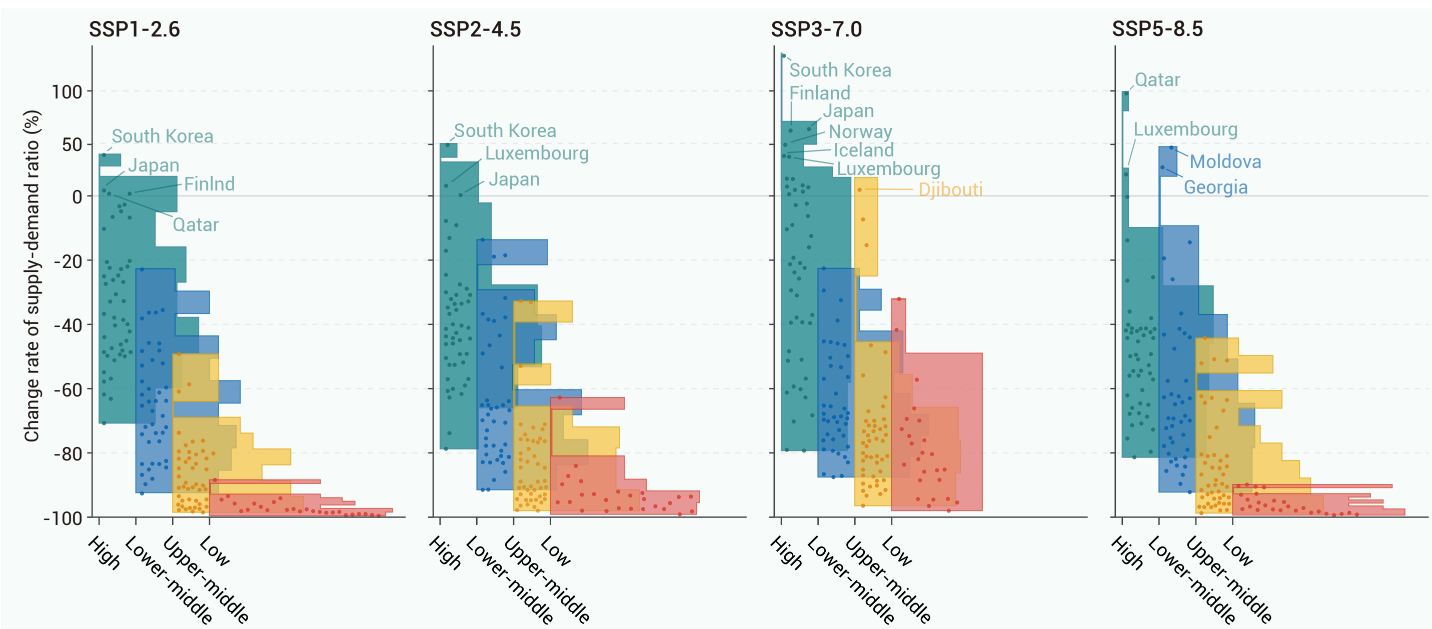

Figure 7. Projected change in supply-demand ratio across countries of different income levels Color indicates countries categorized by income level. Point represents the country-level change rates of supply-demand ratio, and histogram displays point density.

2 billion buildings (Figure S15), and the estimated rooftop area is higher than the two previous studies while showing a spatial distribution generally consistent with ref.[17] at macro-region level. Meanwhile, our estimated rooftop area compares well with selected studies at regional, national, and city levels (Table S9). In addition to reliable rooftop area estimation, we employ a technically rigorous photovoltaic performance model to precisely assess the capacity factor considering specific climatic conditions and updated technological parameters. This contrasts with ref.[3] that uses a historical average yield dataset (in kWh/kWp/month) dating as far back as 1994 despite recent dramatic changes,[51] and ref.[17] that relies on oversimplified empirical formulas. Our estimated capacity factor and its future changes (Figure S16) show broad agreement with recent work in both magnitude and distribution.[12,13,19,52,53] Based on the accurate RPV potential assessment, our study fills a critical gap in evaluating the combined effects of future urbanization and climate change on RPV potential, contributing to a better understanding of the potential role of RPVs in global and regional electricity systems.

Constrained rooftop solar viability in lower-income countries

Our projections demonstrate that urban expansion can significantly enhance worldwide RPV potential during the 21st century (Figures 2-3), whereas the prevalent trend of urban densification may lead to a decline in per capita size (Figures 4-5). We call for more attention to low- and lower-middle-income groups of countries undergoing rapid urbanization, where urban expansion could boost RPV potential by over 20%. Nevertheless, this growth is likely insufficient to counteract the dilution from rising population and electricity demand, especially in low-income group where per capita RPV potential decline across all scenarios. Moreover, climate change can also exert notable impacts on RPV potential (Figure 3). Lower-income groups are exposed to stronger negative impacts from high emissions than wealthier groups, as climate-induced RPV potential losses will offset a large fraction (> 20%) of the gains associated with urban expansion. Despite the climatic conditions under low-emissions scenario favoring RPV potential in most of the world, low-income group can only benefit marginally from this. In line with growing electricity demand, RPV potential supply in low-income countries will likely soon shift from substantial surpluses to deficits (Figure 6). In conclusion, our findings suggest that combined effects of urbanization and climate change may jeopardize the long-term prospects of low-income countries for integrating RPVs into electricity systems.

Low-income countries bear a disproportionate future burden, related to not only the projected quantities of RPV potential but also their reliance on the benefits offered by RPVs. In contrast to high-income countries having diverse and stable energy supply, low-income countries are far more disadvantageous in access to electricity. The development in low-income countries requires fast expanding infrastructure and prioritizes the most cost-effective power resources. Previous research indicated that renewables can be cost-competitive for universal electricity access in low-income countries, especially those in Africa.[5,54-56] Hydroelectricity is currently the primary renewables for African countries,[57] but its catchment-wide social and environmental risks have become critical concerns in these countries.[58,59] RPVs present a more reliable and environmentally-friendly solution,[57,60] while also offering additional benefits like job creation and economic development.[61,62] However, its desirability would be compromised without timely planning in response to urbanization and climate change. This is especially the case under high-emissions scenarios, where widespread capacity factor reductions quantitatively offset the gains from urban expansion and qualitatively increase unit costs of production.[63] Additionally, atmospheric pollutants and dust deposition associated with high emissions[21] will raise the costs of maintenance and operations.[64] These undesirable consequences would undermine RPV affordability and deployment willingness, potentially driving households in low-income countries to revert to fossil fuels, which in turn aggravates emissions and environmental pollution.[65] Overall, our analyses underscore the urgent need for climate and socioeconomic strategies to prevent the uneven changes in RPV potential exacerbating electricity access inequalities, especially considering that ensuring widely accessible renewables is pivotal for an equitable and just clean energy transition globally.[66]

Policy implications

In light of the contrasting climate impacts on global RPV potential between low-/intermediate- and high-emissions scenarios, it is advisable to accelerate the near-term deployment of renewables like RPVs, so as to reinforce the virtuous cycle between emission reduction and RPV potential growth. Otherwise, prioritizing economic development at the expense of emissions may trap low-income countries in a vicious cycle as discussed above, or worse, cause irreversible adverse climate impacts. The impending urban expansion offers an opportunity to optimize RPV potential and facilitate RPV deployment. Specifically, RPVs can be integrated into the initial design of newly constructed buildings, such as optimizing building's shape to maximize solar exposure and available area for RPV installation, thereby enhancing generation efficiency and rooftop availability. Here we document global and regional RPV potential and their corresponding supply-demand ratios based on varying rooftop availability to provide a quantifiable reference (Tables S7 & S10). Moreover, utilizing RPVs as building envelopes can provide additional cost savings and, in certain countries, greater financial incentives.[67] Also, incorporating aesthetic considerations in design process would promote public acceptance and marketability of RPVs, especially in urban environments.[68] Similar building-related strategies have recently been implemented by the European Union through regulations regarding mandatory RPV installation in new construction.[49] Meanwhile, ongoing technological progress in photovoltaics will likely improve their solar-to-electric conversion efficiency.[69] By supplementing two sets of RPV potential assessments using more advanced photovoltaic modules (Table S5), we present that RPV potential could double if the conversion efficiency of current mainstream silicon-based modules reaches its theoretical limit. Notwithstanding, technological innovation distributes unevenly and often excludes vulnerable populations from its benefits,[70] for which overreliance on advanced technologies to compensate for high-emissions-induced losses should be avoided as it may accentuate inequalities. Since industrialized countries are the lead innovators in photovoltaics and meanwhile the world's major emitters,[71,72] they should actively accelerate their RPV deployment while prioritizing financial and technical transfers for lower-income countries to advance global energy transition. If proactive actions are taken in the coming decades, the disproportionate impacts we report on lower-income countries could be mitigated.

Limitations

Our study should be interpreted in recognition of some caveats. Following previous studies,[2-4,12-14,16,17,19] we simplify several complicated factors for global-scale assessments, such as uniform assumptions regarding rooftop availability and system configurations (see Materials and Methods). The presented results offer a valuable global insight, but region-specific RPV deployment requires more sophisticated investigations to address the contextual challenges. For example, complex urban environments pose multifaceted constraints concerning issues such as superstructures for different types of buildings,[73] restrictions on modifying heritage architecture,[74] household economic disparities influencing technology accessibility,[75] and disputes over private RPV installation occupying public roof space.[76] Nevertheless, large-scale RPV deployment can alter the energy balance of buildings as well as the urban surface, hence modifying urban climate and related energy demand.[77] Our assessments exclude these feedback effects due to their high uncertainty and sometimes contradictory published findings because of many complex interaction mechanisms.[77-81] Furthermore, RPVs alone, albeit persistently covering much of the electricity demand, may struggle to provide sufficient and stable electricity for growing future needs, particularly given the intensified peak fluctuations associated with urban densification.[82] Future research should thus explore synergistic renewable portfolios for better grid stability, where our RPV potential assessments could provide valuable information. Despite these limitations, as a pioneering effort to understand how urbanization and climate change jointly affect RPV potential globally, our analyses help policymakers and stakeholders better allocate resources and make concerted global efforts on climate mitigation.

REFERENCES

1. Wang Y., Wang R., Tanaka K., et al. (2025). Global spatiotemporal optimization of photovoltaic and wind power to achieve the Paris agreement targets. *Nat. Commun.* **16**:2127. DOI:10.1038/s41467-025-57292-w
2. Martinopoulos G. (2020). Are rooftop photovoltaic systems a sustainable solution for Europe. *A life cycle impact assessment and cost analysis. Appl. Energy* **257**:114035. DOI:10.1016/j.apenergy.2019.114035
3. Joshi S., Mittal S., Holloway P., et al. (2021). High resolution global spatiotemporal assessment of rooftop solar photovoltaics potential for renewable electricity generation. *Nat. Commun.* **12**:5738. DOI:10.1038/s41467-021-25720-2
4. Zhang Z., Chen M., Zhong T., et al. (2023). Carbon mitigation potential afforded by rooftop photovoltaic in China. *Nat. Commun.* **14**:2347. DOI:10.1038/s41467-023-38079-3
5. Barasa M., Bogdanov D., Oyewo A. S., et al. (2018). A cost optimal resolution for Sub-Saharan Africa powered by 100% renewables in 2030. *Renew. Sust. Energ. Rev.* **92**:440–457. DOI:10.1016/j.rser.2018.04.110
6. Zope R. Rooftop solar PV market size, share, growth, and regional forecast, 2025-2032. https://www.persistencemarketresearch.com/market-research/rooftop-solar-pv-market.asp
7. Assouline D., Mohajeri N. and Scartezzini J.-L. (2017). Quantifying rooftop photovoltaic solar energy potential: A machine learning approach. *Sol. Energy* **141**:278–296. DOI:10.1016/j.solener.2016.11.045
8. Frolking S., Mahtta R., Milliman T., et al. (2024). Global urban structural growth shows a profound shift from spreading out to building up. *Nat. Cities* **1**:555–566. DOI:10.1038/s44284-024-00100-1
9. Liu X., Wu X., Li X., et al. (2025). Global mapping of three-dimensional urban structures reveals escalating utilization in the vertical dimension and pronounced building space inequality. *Engineering* **47**:86–99. DOI:10.1016/j.eng.2024.01.025
10. Skoplaki E. and Palyvos J. A. (2009). On the temperature dependence of photovoltaic module electrical performance: A review of efficiency/power correlations. *Sol. Energy* **83**:614–624. DOI:10.1016/j.solener.2008.10.008
11. Chenni R., Makhlouf M., Kerbache T., et al. (2007). A detailed modeling method for photovoltaic cells. *Energy* **32**:1724–1730. DOI:10.1016/j.energy.2006.12.006
12. Chen X., Mao H., Cheng N., et al. (2024). Climate change impacts on global photovoltaic variability. *Appl. Energy* **374**:124087. DOI:10.1016/j.apenergy.2024.124087
13. Lei Y., Wang Z., Wang D., et al. (2023). Co-benefits of carbon neutrality in enhancing and stabilizing solar and wind energy. *Nat. Clim. Change* **13**:693–700. DOI:10.1038/s41558-023-01692-7
14. Isaza A., Kay M., Evans J. P., et al. (2023). Maximizing photovoltaic potential and minimizing costs in a future warmer climate: The role of atmospheric aerosols and greenhouse gas emissions. *Renew. Energ.* **219**:119561. DOI:10.1016/j.renene.2023.119561
15. Wild M., Folini D., Henschel F., et al. (2015). Projections of long-term changes in solar radiation based on CMIP5 climate models and their influence on energy yields of photovoltaic systems. *Sol. Energy* **116**:12–24. DOI:10.1016/j.solener.2015.03.039
16. Crook J. A., Jones L. A., Forster P. M., et al. (2011). Climate change impacts on future

photovoltaic and concentrated solar power energy output. *Energ. Environ. Sci.* **4**:3101–3109. DOI:10.1039/C1EE01495A

17. Zhang Z., Qian Z., Chen M., et al. (2025). Worldwide rooftop photovoltaic electricity generation may mitigate global warming. *Nat. Clim. Change* **15**:393–402. DOI:10.1038/s41558-025-02276-3
18. O'Neill B. C., Kriegler E., Riahi K., et al. (2014). A new scenario framework for climate change research: the concept of shared socioeconomic pathways. *Clim. Change* **122**:387–400. DOI:10.1007/s10584-013-0905-2
19. Lu N., Yao L., Qin J., et al. (2022). High emission scenario substantially damages China's photovoltaic potential. *Geophys. Res. Lett.* **49**:e2022GL100068. DOI:10.1029/2022GL100068
20. Masson-Delmotte V., Zhai P., Pörtner H.-O., et al. (2018). Global warming of 1.5 C: IPCC special report on impacts of global warming of 1.5 C above pre-industrial levels in context of strengthening response to climate change, sustainable development, and efforts to eradicate poverty. https://www.ipcc.ch/sr15/
21. O'Neill B. C., Carter T. R., Ebi K., et al. (2020). Achievements and needs for the climate change scenario framework. *Nat. Clim. Change* **10**:1074–1084. DOI:10.1038/s41558-020-00952-0
22. van Vuuren D. P., Edmonds J., Kainuma M., et al. (2011). The representative concentration pathways: An overview. *Clim. Change* **109**:5. DOI:10.1007/s10584-011-0148-z
23. Sirko W., Kashubin S., Ritter M., et al. (2021). Continental-scale building detection from high resolution satellite imagery. *arXiv preprint arXiv:2107.12283*. DOI:10.48550/arXiv.2107.12283
24. Heris M. P., Foks N. L., Bagstad K. J., et al. (2020). A rasterized building footprint dataset for the United States. *Sci. Data* **7**:207. DOI:10.1038/s41597-020-0542-3
25. Zhang Z., Qian Z., Zhong T., et al. (2022). Vectorized rooftop area data for 90 cities in China. *Sci. Data* **9**:66. DOI:10.1038/s41597-022-01168-x
26. Chen G., Li X., Liu X., et al. (2020). Global projections of future urban land expansion under shared socioeconomic pathways. *Nat. Commun.* **11**:537. DOI:10.1038/s41467-020-14386-x
27. Lloyd C. T., Chamberlain H., Kerr D., et al. (2019). Global spatio-temporally harmonised datasets for producing high-resolution gridded population distribution datasets. *Big Earth Data* **3**:108–139. DOI:10.1080/20964471.2019.1625151
28. Li M., Zhou B.-B., Gao M., et al. (2022). Spatiotemporal dynamics of global population and heat exposure (2020–2100): Based on improved SSP-consistent population projections. *Environ. Res. Lett.* **17**:094007. DOI:10.1088/1748-9326/ac8755
29. Meijer J. R., Huijbregts M. A. J., Schotten K. C. G. J., et al. (2018). Global patterns of current and future road infrastructure. *Environ. Res. Lett.* **13**:064006. DOI:10.1088/1748-9326/aabd42
30. Hastings D. A. and Dunbar P. (1998). Development & assessment of the global land one-km base elevation digital elevation model (GLOBE). *Int. Soc. Photogramm. Remote Sens.* **4**:218-221. https://www.isprs.org/proceedings/XXXII/part4/hastings54.pdf
31. Beck H. E., Zimmermann N. E., McVicar T. R., et al. (2018). Present and future Köppen-Geiger climate classification maps at 1-km resolution. *Sci. Data* **5**:180214. DOI:10.1038/sdata.2018.214
32. Thrasher B., Wang W., Michaelis A., et al. (2022). NASA global daily downscaled projections, CMIP6. *Sci. Data* **9**:262. DOI:10.1038/s41597-022-01393-4
33. World Bank Group (2019). Global solar atlas 2.0: Technical report (English). http://documents.worldbank.org/curated/en/529431592893043403
34. Dobos A. P. (2012). An improved coefficient calculator for the california energy commission 6 parameter photovoltaic module model. *J. Sol. Energy Eng.* **134**:021011. DOI:10.1115/1.4005759
35. Keiner D., Gulagi A. and Breyer C. (2023). Energy demand estimation using a pre-processing macro-economic modelling tool for 21st century transition analyses. *Energy* **272**:127199. DOI:10.1016/j.energy.2023.127199
36. Chen T. and Guestrin C. (2016). XGBoost: A scalable tree boosting system. Krishnapuram, B., Shah M., Smola A., et al. (eds). Proceedings of the 22nd ACM SIGKDD International Conference on Knowledge Discovery and Data Mining (Association for Computing Machinery), pp:785–794. DOI: 10.1145/2939672.2939785
37. Prokhorenkova L., Gusev G., Vorobev A., et al. (2018). CatBoost: Unbiased boosting with categorical features. Bengio, S., Wallach H. M., Larochelle H., et al. (eds). NIPS'18: Proceedings of the 32nd international conference on neural information processing systems (Curran Associates Inc.), pp:6639–6649. DOI: 10.5555/3327757.3327770
38. Ke G., Meng Q., Finley T., et al. (2017). LightGBM: A highly efficient gradient boosting decision tree. Luxburg U. V., Guyon I., Bengio S., et al. (eds). NIPS'17: Proceedings of the 31st international conference on neural information processing systems (Curran Associates Inc.), pp:3149–3157. DOI: 10.5555/3294996.3295074
39. Brenning A. (2012). Spatial cross-validation and bootstrap for the assessment of prediction rules in remote sensing: The R package sperrorest. *2012 IEEE IGARSS* DOI: 10.1109/IGARSS.2012.6352393
40. Mohajeri N., Assouline D., Guiboud B., et al. (2018). A city-scale roof shape classification using machine learning for solar energy applications. *Renew. Energ.* **121**:81–93. DOI:10.1016/j.renene.2017.12.096
41. Andrews R. W., Stein J. S., Hansen C., et al. (2014). Introduction to the open source PVLIB for python photovoltaic system modelling package. *2014 IEEE 40th PVSC* DOI: 10.1109/PVSC.2014.6925501
42. Müller J., Folini D., Wild M., et al. (2019). CMIP-5 models project photovoltaics are a no-regrets investment in Europe irrespective of climate change. *Energy* **171**:135–148. DOI:10.1016/j.energy.2018.12.139
43. Ineichen P., Perez R., Seal R., et al. (1992). Dynamic global-to-direct irradiance conversion models. *Ashrae Trans.* **98**:354-369. https://www.researchgate.net/publication/279868352_Dynamic_global-to-direct_irradiance_conversion_models
44. Reda I. and Andreas A. (2004). Solar position algorithm for solar radiation applications. *Sol. Energy* **76**:577–589. DOI:10.1016/j.solener.2003.12.003
45. Hay J. E. and Davies J. A. (1980). Calculations of the solar radiation incident on an inclined surface. Hay, J.E. and Won T. K. (eds). Proceedings of first Canadian solar radiation data workshop (Ministry of Supply and Services), pp:59–72. https://archive.org/details/proceedingsfirst00cana
46. Kratochvil J. A., Boyson W. E. and King D. L. (2004). Photovoltaic array performance model. DOI: 10.2172/919131
47. Galen L. B., Naïm R. D., Eric O. S., et al. (2022). Tracking the Sun: Pricing and design trends for distributed photovoltaic systems in the United States, 2022 Edition. https://emp.lbl.gov/publications/tracking-sun-pricing-and-design-1
48. Bhattacharya S. and John S. (2019). Beyond 30% conversion efficiency in silicon solar cells: A numerical demonstration. *Sci. Rep.* **9**:12482. DOI:10.1038/s41598-019-48981-w
49. European Commission (2022). EU solar energy strategy. https://eur-lex.europa.eu/legal-content/EN/TXT/HTML/?uri=CELEX:52022DC0221
50. Bauer N., Calvin K., Emmerling J., et al. (2017). Shared socio-economic pathways of the energy sector–quantifying the narratives. *Global Environ. Chang.* **42**:316–330. DOI:10.1016/j.gloenvcha.2016.07.006
51. Miller L. M. and Keith D. W. (2018). Observation-based solar and wind power capacity factors and power densities. *Env. Res. Lett.* **13**:104008. DOI:10.1088/1748-9326/aae102
52. Bódis K., Kougias I., Jäger-Waldau A., et al. (2019). A high-resolution geospatial assessment of the rooftop solar photovoltaic potential in the European Union. *Renew. Sust. Energ. Rev.* **114**:109309. DOI:10.1016/j.rser.2019.109309
53. Tang Q., Wu J., Xiao J., et al. (2021). Assessment of global solar resource development. *Glob. Energy Interconnect.* **4**:453–464. DOI:10.1016/j.gloei.2021.11.002
54. van der Zwaan B., Kober T., Longa F. D., et al. (2018). An integrated assessment of pathways for low-carbon development in Africa. *Energy Policy* **117**:387–395. DOI:10.1016/j.enpol.2018.03.017
55. Ram M., Bogdanov D., Aghahosseini A., et al. (2022). Global energy transition to 100% renewables by 2050: Not fiction, but much needed impetus for developing economies to leapfrog into a sustainable future. *Energy* **246**:123419. DOI:10.1016/j.energy.2022.123419
56. Szabó S., Pinedo Pascua I., Puig D., et al. (2021). Mapping of affordability levels for photovoltaic-based electricity generation in the solar belt of sub-Saharan Africa, East Asia and South Asia. *Sci. Rep.* **11**:3226. DOI:10.1038/s41598-021-82638-x
57. Peters R., Berlekamp J., Kabiri C., et al. (2024). Sustainable pathways towards universal renewable electricity access in Africa. *Nat. Rev. Earth Env.* **5**:137–151. DOI:10.1038/s43017-023-00501-1
58. Polimeni J. M., Iorgulescu R. I. and Chandrasekara R. (2014). Trans-border public health vulnerability and hydroelectric projects: The case of Yali Falls Dam. *Ecol. Econ.* **98**:81–89. DOI:10.1016/j.ecolecon.2013.12.013
59. Zarfl C. and Lucía A. (2018). The connectivity between soil erosion and sediment entrapment in reservoirs. *Curr. Opin. Environ. Sci. Health* **5**:53–59. DOI:10.1016/j.coesh.2018.05.001
60. Arnold W., Giuliani M. and Castelletti A. (2024). Floating photovoltaics may reduce the risk of hydro-dominated energy development in Africa. *Nat. Energy* **9**:602–611. DOI:10.1038/s41560-024-01510-0
61. Ram M., Aghahosseini A. and Breyer C. (2020). Job creation during the global energy transition towards 100% renewable power system by 2050. *Technol. Forecast. Soc.* **151**:119682. DOI:10.1016/j.techfore.2019.06.008
62. Adams S., Klobodu E. K. M. and Apio A. (2018). Renewable and non-renewable energy, regime type and economic growth. *Renew. Energ.* **125**:755–767. DOI:10.1016/j.renene.2018.02.135
63. Staffell I. and Green R. (2014). How does wind farm performance decline with age. *Renew. Energ.* **66**:775–786. DOI:10.1016/j.renene.2013.10.041
64. Kosmadakis I. E., Elmasides C., Koulinas G., et al. (2021). Energy unit cost assessment of six photovoltaic-battery configurations. *Renew. Energ.* **173**:24–41. DOI:10.1016/j.renene.2021.03.010
65. Solomon C. G., Salas R. N., Malina D., et al. (2022). Fossil-fuel pollution and climate change—A new NEJM group series. *NEJM Catalyst* **3**:7. DOI. doi:10.1056/CAT.22.0186
66. Carley S. and Konisky D. M. (2020). The justice and equity implications of the clean energy transition. *Nat. Energy* **5**:569–577. DOI:10.1038/s41560-020-0641-6
67. Ding L., Zhu Y., Zheng L., et al. (2023). What is the path of photovoltaic building (BIPV

or BAPV) promotion. -The perspective of evolutionary games. *Appl. Energ.* 340:121033. DOI:10.1016/j.apenergy.2023.121033
68. Awuku S. A., Bennadji A., Muhammad-Sukki F., et al. (2021). Myth or gold. The power of aesthetics in the adoption of building integrated photovoltaics (BIPVs). *Energy Nexus* 4:100021. DOI:10.1016/j.nexus.2021.100021
69. Fazal M. A. and Rubaiee S. (2023). Progress of PV cell technology: Feasibility of building materials, cost, performance, and stability. *Sol. Energy* 258:203–219. DOI:10.1016/j.solener.2023.04.066
70. Sovacool B. K., Newell P., Carley S., et al. (2022). Equity, technological innovation and sustainable behaviour in a low-carbon future. *Nat. Hum. Behav.* 6:326–337. DOI:10.1038/s41562-021-01257-8
71. Gao X. and Zhang Y. (2022). What is behind the globalization of technology. Exploring the interplay of multi-level drivers of international patent extension in the solar photovoltaic industry. *Renew. Sust. Energ. Rev.* 163:112510. DOI:10.1016/j.rser.2022.112510
72. Fyson C. L., Baur S., Gidden M., et al. (2020). Fair-share carbon dioxide removal increases major emitter responsibility. *Nat. Clim. Change* 10:836–841. DOI:10.1038/s41558-020-0857-2
73. Li Q., Krapf S., Mou L., et al. (2024). Deep learning-based framework for city-scale rooftop solar potential estimation by considering roof superstructures. *Appl. Energ.* 374:123839. DOI:10.1016/j.apenergy.2024.123839
74. Del Hierro López I. and Olivieri L. (2025). Comprehensive review of building-integrated photovoltaics in the renovation of heritage buildings. *J. Build. Eng.* 108:112883. DOI:10.1016/j.jobe.2025.112883
75. Sunter D. A., Castellanos S. and Kammen D. M. (2019). Disparities in rooftop photovoltaics deployment in the United States by race and ethnicity. *Nat. Sustain.* 2:71–76. DOI:10.1038/s41893-018-0204-z
76. Poshnath A., Rismanchi B. and Rajabifard A. (2023). Adoption of Renewable Energy Systems in common properties of multi-owned buildings: Introduction of 'Energy Entitlement'. *Energ. Policy* 174:113465. DOI:10.1016/j.enpol.2023.113465
77. Kapsalis V., Maduta C., Skandalos N., et al. (2024). Critical assessment of large-scale rooftop photovoltaics deployment in the global urban environment. *Renew. Sust. Energ. Rev.* 189:114005. DOI:10.1016/j.rser.2023.114005
78. Chen B., Wang W., You Y., et al. (2023). Influence of rooftop mitigation strategies on the thermal environment in a subtropical city. *Urban. Clim.* 49:101450. DOI:10.1016/j.uclim.2023.101450
79. Zhang H., Luo M., Pei T., et al. (2023). Unequal urban heat burdens impede climate justice and equity goals. *The Innovation* 4:100488. DOI:10.1016/j.xinn.2023.100488
80. Maurer B., Lienert J. and Cook L. M. (2023). Comparing PV-green and PV-cool roofs to diverse rooftop options using decision analysis. *Build. Environ.* 245:110922. DOI:10.1016/j.buildenv.2023.110922
81. Zonato A., Martilli A., Gutierrez E., et al. (2021). Exploring the effects of rooftop mitigation strategies on urban temperatures and energy consumption. *J. Geophys. Res. Atmos.* 126:e2021JD035002. DOI:10.1029/2021JD035002
82. Perera A. T. D., Javanroodi K., Mauree D., et al. (2023). Challenges resulting from urban density and climate change for the EU energy transition. *Nat. Energy* 8:397–412. DOI:10.1038/s41560-023-01232-9

FUNDING AND ACKNOWLEDGMENTS

The research was supported by the National Natural Science Foundation of China (Grant No. 42322110 and 42271415). The funders had no role in study design, data collection and analysis, decision to publish, or preparation of the manuscript.

AUTHOR CONTRIBUTIONS

Y.C., Y.Y., and X.Liu conceptualized the research design; J.C. performed the analysis; J.C. and Y.C. wrote the draft. All authors contributed to the interpretation of the results and the writing of the paper. All authors contributed to the manuscript and approved the final version.

DECLARATION OF INTERESTS

The authors declare no competing interests.

DATA AND CODE AVAILABILITY

The dataset used in this analysis is publicly available. The building footprints are collected from Google Open Buildings V2 (https://sites.research.google/open-buildings/), Microsoft Building Footprints (https://github.com/microsoft/GlobalMLBuildingFootprints), and ref.[25]; the urban land maps for the baseline year 2015 and the SSP scenarios can be accessed via https://doi.pangaea.de/10.1594/PANGAEA.905890; the 2015 gridded population map is obtained from WorldPop (https://hub.worldpop.org/geodata/listing?id=75) and the SSP projections can be accessed via https://www.geosimulation.cn/FPOP.html; the road network data can be accessed via https://www.globio.info/download-grip-dataset; the DEM data can be accessed via https://www.ngdc.noaa.gov/mgg/topo/globe.html; the Köppen-Geiger climate classification can be accessed via https://doi.org/10.6084/m9.figshare.6396959; the NEX-GDDP-CMIP6 climate projections can be accessed via https://www.nccs.nasa.gov/services/data-collections/land-based-products/nex-gddp-cmip6; the optimal tilt angle from Global Solar Atlas can be accessed via https://globalsolaratlas.info/download/world; the California Energy Commission photovoltaic module database can be accessed via https://github.com/NREL/SAM/tree/develop/samples/CEC%20Module%20and%20Inverter%20Libraries; and the electricity demand data can be obtained from ref.[35]. The delineation of administrative areas follows the definition of the Global Administrative Areas 3.4 Data Set (https://gadm.org/). The other data and code supporting the analysis in this paper are available from the corresponding author upon reasonable request.

SUPPLEMENTAL INFORMATION

It can be found online at https://doi.org/10.59717/j.xinn-geo.2026.100222.